Research Square

Preprints are preliminary reports that have not undergone peer review.
They should not be considered conclusive, used to inform clinical practice,
or referenced by the media as validated information.

TLR5 signaling amplifies airway epithelial cell responses to influenza through a MyD88–JAK1 crosstalk

Ignacio Caballero

ignacio.caballero-posadas@inrae.fr

INRAE

Elaa Chkhaydem

Isabelle Fleurot

UMR ISP, INRAE https://orcid.org/0000-0002-0728-251X

Iuliia Parfenova

Vanaique Guillory

UMR ISP, INRAE

Emmanuel Kut

UMR ISP, INRAE

Celine Barc

Jérémy Pezant

Stefanie Ebersberger

Isabelle Seufert

Laetitia Gaigeard

Marie Couralet

Gaëlle Simon

Pascal Barbry

Université Côte d'Azur, CNRS, Inserm https://orcid.org/0000-0001-9632-6483

jean-claude sirard

Ferdinand Roesch

UMR ISP, INRAE

Sascha Trapp

INRAE https://orcid.org/0000-0002-2735-0217

Article

Keywords:

Posted Date: November 11th, 2026

DOI: https://doi.org/10.21203/rs.3.rs-11049330/v1

License: This work is licensed under a Creative Commons Attribution 4.0 International License.
Read Full License

Additional Declarations: Yes there is potential Competing Interest. Jean-Claude Sirard is the inventor of the patents WO2009156405, WO2011161491, and WO2015011254 that describes the use of recombinant flagellin as biologic against infectious diseases and the patent WO2023275292 on the formulation of FLAMOD. All other authors declare they have no competing interests.

TLR5 signaling amplifies airway epithelial cell responses to influenza through a MyD88–JAK1 crosstalk

Authors

Elaa Chkhaydem[1], Isabelle Fleurot[1], Iuliia Parfenova[2], Vanaique Guillory[1], Emmanuel Kut[1], Celine Barc[3], Jérémy Pezant[3], Stefanie Ebersberger[4], Isabelle Seufert[4], Laetitia Gaigeard[5], Marie Couralet[5], Gaëlle Simon[6], Pascal Barbry[5,7,8], Jean-Claude Sirard[9], Ferdinand Roesch[1], Sascha Trapp[1], Ignacio Caballero[1,10,*].

Affiliations

[1]Infectiologie et Santé Publique, UMR1282, INRAE, University of Tours, 37380 Nouzilly, France.
[2]d-fine AG, Zurich, Switzerland.
[3]INRAE, UE1277 PFIE, Nouzilly, France.
[4]d-fine GmbH, Frankfurt am Main, Germany.
[5]Université Côte d'Azur, CNRS, INSERM, Institut de Pharmacologie Moléculaire et Cellulaire, 06560 Sophia Antipolis, France.
[6]Swine Virology, Innovation and Genomics Unit, Ploufragan-Plouzané-Niort Laboratory, French Agency for Food, Environmental and Occupational Health and Safety (ANSES), Ploufragan, France.
[7]3IA-Côte d'Azur, 06560 Sophia Antipolis, France.
[8]IHU Respirera, 06560 Sophia Antipolis, France.
[9]Univ. Lille, CNRS, INSERM, CHU Lille, Institut Pasteur de Lille, U1019 – UMR9017 - CIIL - Center for Infection and Immunity of Lille, F-59000 Lille, France.
[10]Toxalim, Université de Toulouse, INRAE, ENVT, EI-Purpan, Toulouse, France.

***Corresponding author:** ignacio.caballero-posadas@inrae.fr

Abstract

Influenza vaccines and antivirals are compromised by viral evolution, underscoring the need for host-directed strategies that provide broad, strain-independent protection. While flagellin, a Toll-like receptor 5 (TLR5) agonist, has an established role in shielding against respiratory bacterial infection, its role in shaping antiviral defenses in the airway epithelium remains poorly understood. Using porcine bronchial epithelial cells and pigs infected with swine influenza A virus (SIAV), we show that TLR5 activation sensitizes cells to type I interferon (IFN). Flagellin lowered the IFN concentration required for STAT2 activation, amplifying interferon-stimulated gene expression, and suppressing viral replication. This effect required IFN signaling and MyD88, and coincided with a flagellin-induced MyD88–JAK1 interaction. In SIAV-infected pigs, a single administration of flagellin was sufficient to heighten IFN responsiveness and to mitigate disease severity. These findings reveal a novel crosstalk between TLR5 and IFN pathways, offering a strain-independent route to boost antiviral protection.

Keywords: Swine Influenza, Flagellin, Innate Immunity, TLR5

INTRODUCTION

Swine influenza A viruses (SIAV) are major viral pathogens within the porcine respiratory disease complex (PRDC)[1], a multifactorial syndrome that compromises respiratory health and productivity in pig farms. Beyond the acute respiratory disease, SIAV infection impairs lung function and predisposes pigs to secondary bacterial infections, substantially increasing economic losses[2]. In addition, SIAV pose a significant zoonotic risk, as pigs can act as "mixing reservoirs" that facilitate reassortment and transmission of influenza A viruses between avian and mammalian hosts[3,4].

Vaccination remains the principal control strategy, but its effectiveness is limited by antigenic drift of circulating field viruses[5,6]. Antiviral drugs for human influenza, primarily neuraminidase inhibitors (*e.g.* oseltamivir) and cap-dependent endonuclease inhibitors (*e.g.* baloxavir), have a narrow therapeutic window, suffer from widespread resistance, and are currently not considered as a suitable option by the livestock sector. Consequently, there is a pressing need for strain-independent antiviral approaches that leverage host defenses to benefit both veterinary and human medicine.

An alternative strategy involves immunomodulation through Toll-like Receptor 5 (TLR5), a Pattern Recognition Receptor (PRR) abundantly expressed in airway epithelial cells (AECs), the primary target of influenza A viruses[7]. By modulating host response rather than directly targeting the virus, this host-directed approach offers the potential of strain-independent protection[8–12]. Flagellin, a TLR5 agonist, has emerged as a particularly promising candidate for combating respiratory infections[13], with AECs acting as first responders to flagellin exposure[14,15]. Mucosal administration of flagellin has demonstrated protective activity against respiratory pathogens in several infection models, including bacterial infections in mice[16–18] and pigs[12], as well as influenza[19] and post-influenza pneumococcal infection in murine models[17]. This protective effect is most likely mediated through activation of innate immune pathways in AECs and recruitment of immune effector cells such as neutrophils[10,12].

Our previous work indicates that flagellin also modulates how AECs respond to subsequent pathogen exposure[12], suggesting that TLR5 signaling may shape how AECs respond to SIAV infection. Upon binding to TLR5, flagellin assembles the MyD88-dependent complex ("myddosome"), triggering a signaling cascade that activates the NF-κB pathway[20]. Beyond this canonical pathway, some studies have linked TLR5 to the antiviral response inducing the expression of IFN-β and downstream interferon-stimulated genes (ISGs) in immune cells[21,22]. However, whether TLR5 signaling intersects with the antiviral response in AECs is unknown.

Antibacterial and antiviral defenses are conventionally regarded as distinct. Viral motifs are recognized through PRRs such as RIG-I, MDA-5, TLR3, and TLR7, which converge on NF-κB and interferon regulatory factors 3/7 (IRF3/7) to induce type I interferons (IFN-I) and pro-inflammatory cytokines[7,23]. IFN-I then activates the JAK–STAT pathway, inducing a broad antiviral program through the expression of ISGs[24]. Given the overlapping cellular targets, flagellin may modulate the epithelial response to influenza A virus/SIAV infection. Whether flagellin shapes the antiviral response by inducing IFN-I *de novo* or independently of IFN production remains to be defined.

Here, we investigated how flagellin shapes the antiviral response of porcine AECs to two SIAV strains (H3N2, $H1_{av}N2$). We used FLAMOD, a recombinant flagellin variant ($FliC_{\Delta 174\text{-}400}$)[25] with established immune-stimulatory effects in the pig lungs[11]. FLAMOD enhanced ISG expression and reduced viral titers *in vitro* in a TLR5- and IFN-I dependent manner.

This effect occurred without detectable IFN-I induction, and instead reflected an enhanced cellular sensitivity to IFN-I, uncovering a previously unrecognized layer of antiviral regulation in porcine AECs. *In vivo*, intranasal administration of FLAMOD enhanced pulmonary ISG induction and mitigated influenza-associated lung pathology. These *in vivo* findings corroborate our cellular data, supporting the concept that flagellin-mediated modulation of interferon sensitivity can enhance host resistance to SIAV infection.

RESULTS

FLAMOD treatment induces the expression of anti-viral genes during influenza infection

To determine how FLAMOD modulates the epithelial response to SIAV, we performed microfluidic RT-qPCR profiling on porcine bronchial epithelial cells (T3) infected with an H3N2 strain or left uninfected, followed by FLAMOD treatment 1-hour post-infection (hpi). In non-infected cells, FLAMOD induced the expression of several pro-inflammatory mediators, including *CCL20*, *CXCL2*,*CXCL8*, *CSF2*, and *IL1A*, consistent with our previous observations[12] (Supplementary Figure 1). Hierarchical clustering revealed a distinct group of genes strongly upregulated at 48 hpi in H3N2-infected cells (Figure 1). FLAMOD tended to increase *IFNB* expression and significantly enhanced the expression of multiple ISGs and PRRs, including *DAI, EIF2AK2, IFI16, IFIT1, and RIG-I* (Figure 1B), as well as pro-inflammatory cytokines and chemokines (*CCL20*, *CXCL2, CXCL8*, *IL1A* and *TNFSF10*) (Supplementary Figure 1). FLAMOD-induced upregulation of ISGs occurred only in SIAV-infected cells, indicating that TLR5 signaling further stimulates the virus-induced antiviral transcriptional response.

This effect was conserved across SIAV subtypes. In cells infected with an $H1_{av}N2$ strain, representative of a currently circulating lineage in France[26], FLAMOD significantly increased the expression of *IFITM1*, *ISG15*, *MX1*, and *OAS1* at 48 hpi (Figure 1C). Early induction of *CCL20* and *CXCL8* was also observed at 8 hpi, and both chemokines remained elevated throughout infection (Supplementary Figure 1). Together, these results show that FLAMOD potentiates the antiviral transcriptional program of SIAV-infected porcine AECs.

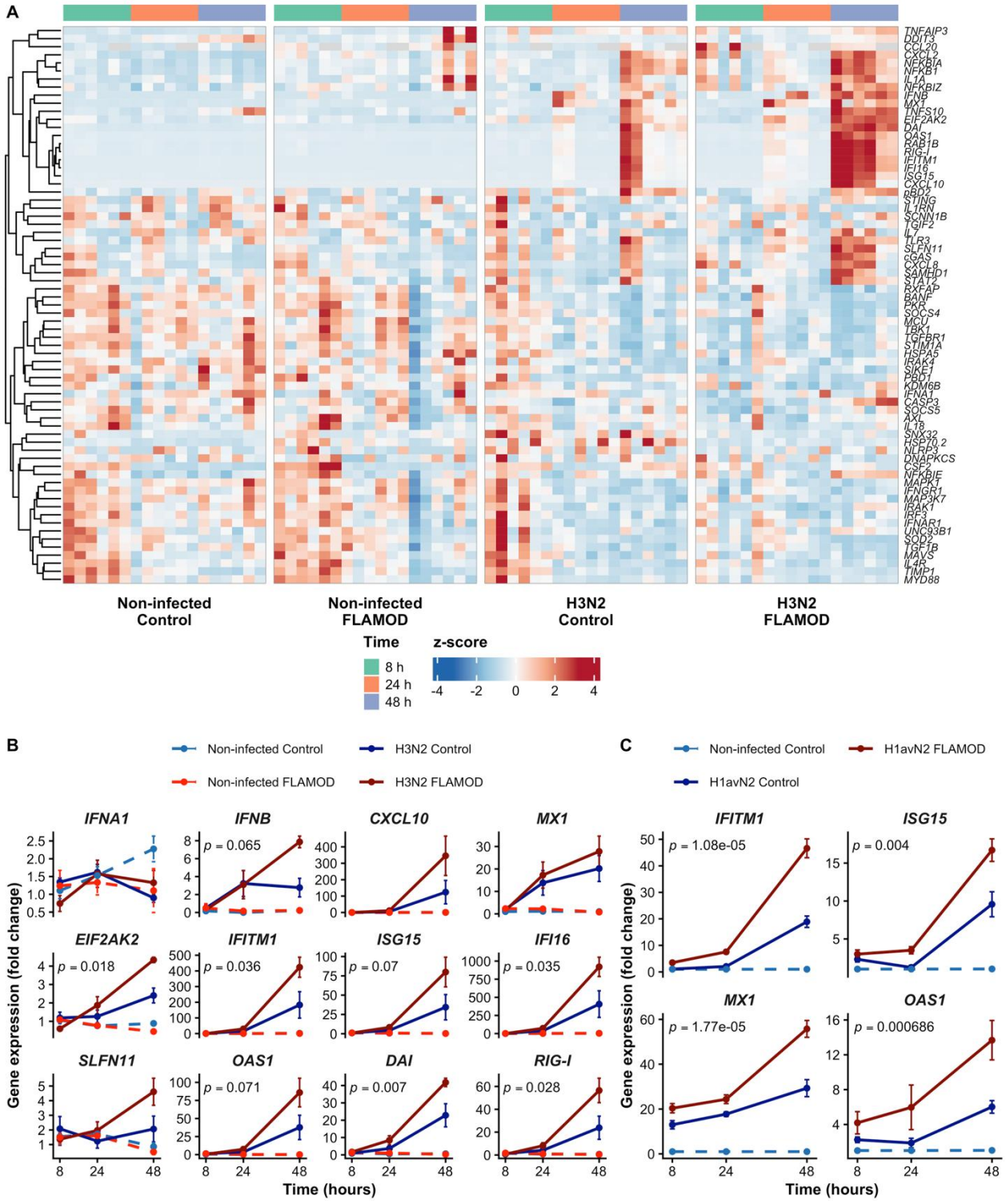


Figure. 1. FLAMOD treatment enhances ISG expression during SIAV infection in porcine bronchial epithelial cells. (A) Heatmap of z-score–normalized gene expression (fold change) across 66 host genes measured by microfluidic RT-qPCR in T3 cells at 8, 24, and 48 hpi. Rows are hierarchically clustered (Euclidean distance, complete linkage) and split into three groups. Each column represents an individual biological replicate (n = 6 per condition). (B) Time-course expression of ISGs and interferon-stimulated PRRs in T3 cells infected with SIAV H3N2 or left uninfected and treated with FLAMOD or vehicle control. (C) ISG expression in T3 cells infected with SIAV H1avN2 and treated with FLAMOD or vehicle control. Data are presented as mean fold change ± SEM (n = 6). p

values indicate the main effect of FLAMOD treatment from a two-way ANOVA (Flagellin × Time) within SIAV-infected cells. Dashed lines represent non-infected groups; solid lines represent SIAV-infected groups.

FLAMOD treatment reduces SIAV titers in porcine airway epithelial cells

Next, we assessed whether these transcriptional changes translated into antiviral activity. We quantified SIAV titers in cells infected with either the H3N2 or $H1_{av}N2$ strain at 8, 24 and 48 hpi. No infectious virus was detected at 8 hpi, and titers increased sharply thereafter. FLAMOD significantly reduced H3N2 titers at 48 hpi (7.9 vs 6.9 $\log_{10}$ $TCID_{50}$/mL in control and FLAMOD-treated cells, respectively) (Figure 2A) and lowered $H1_{av}N2$ titers at both 24 and 48 hpi (Figure 2B). This reduction across two antigenically distinct strains, together with the enhanced ISG expression, indicates that FLAMOD strengthens the epithelial antiviral response and limits SIAV replication.

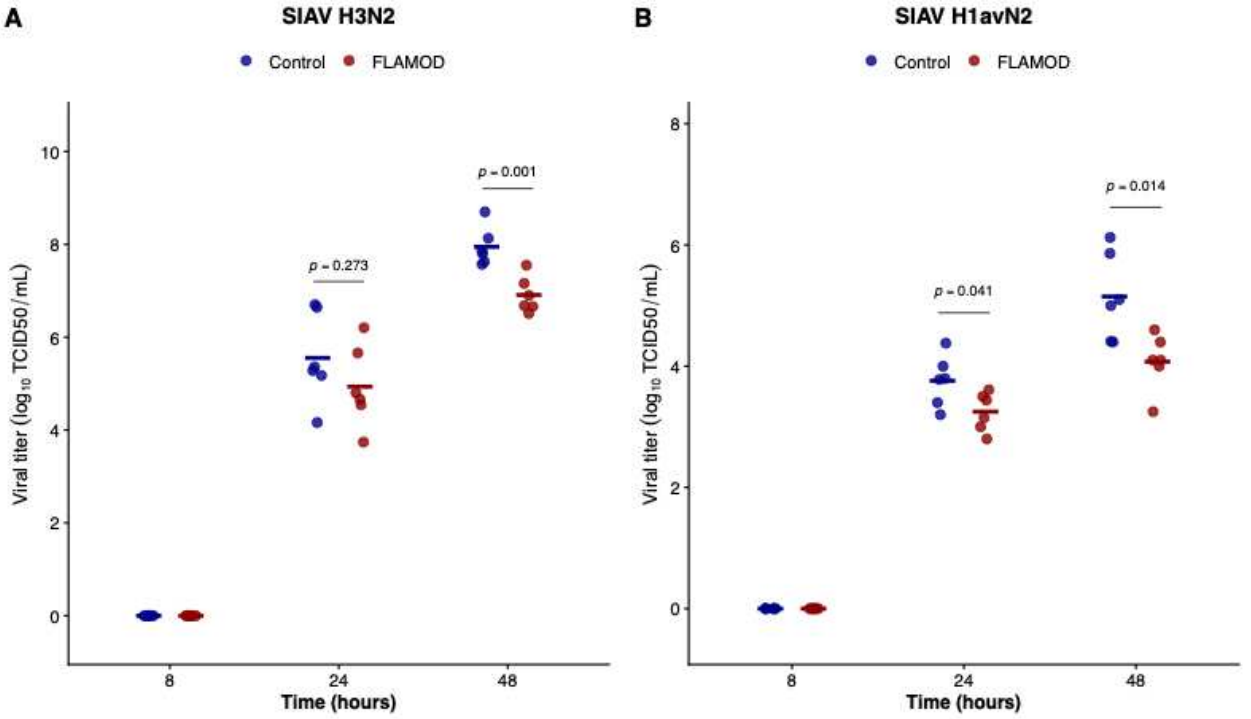


Figure. 2. FLAMOD treatment reduces SIAV replication in porcine bronchial epithelial cells. T3 cells were infected with SIAV H3N2 (A) or SIAV $H1_{av}N2$ (B) and treated with FLAMOD (100 ng/ml) or vehicle control 1 hpi. Supernatants were collected at 8, 24, and 48 hpi and viral titers were determined by TCID50 assay on MDCK cells. Each dot represents an individual biological replicate (n = 6); horizontal bars indicate the mean. p values were calculated using a two-sided Student's t-test comparing FLAMOD-treated and untreated groups at each time point.

FLAMOD-induced ISG expression and antiviral activity require TLR5 signaling

To determine whether the antiviral effect of FLAMOD is mediated solely by TLR5 recognition, we compared the activity of a bioactive flagellin variant ($FliC_{\Delta 3}$) with a TLR5-inactive mutant ($FliC_{\Delta 3.1}$)[27]. Treatment of T3 cells with $FliC_{\Delta 3}$ for 4 h induced a robust upregulation of *CCL20*, *CXCL2* and *CXCL8*, whereas $FliC_{\Delta 3.1}$ failed to elicit any detectable response (Figure 3A). In H3N2-infected cells, $FliC_{\Delta 3}$ significantly increased the expression of antiviral ISGs (*IFITM1*, *ISG15*, *MX1* and *OAS1*), whereas $FliC_{\Delta 3.1}$ had no effect (Figure

3B). Consistent with this lack of ISG induction, FliC$_{\Delta 3.1}$ treatment also failed to reduce viral titers, in contrast to the antiviral effect observed with FliC$_{\Delta 3}$ (Figure 3C). Together, these results demonstrate that TLR5 signaling is essential for both the transcriptional and antiviral effects of flagellin.

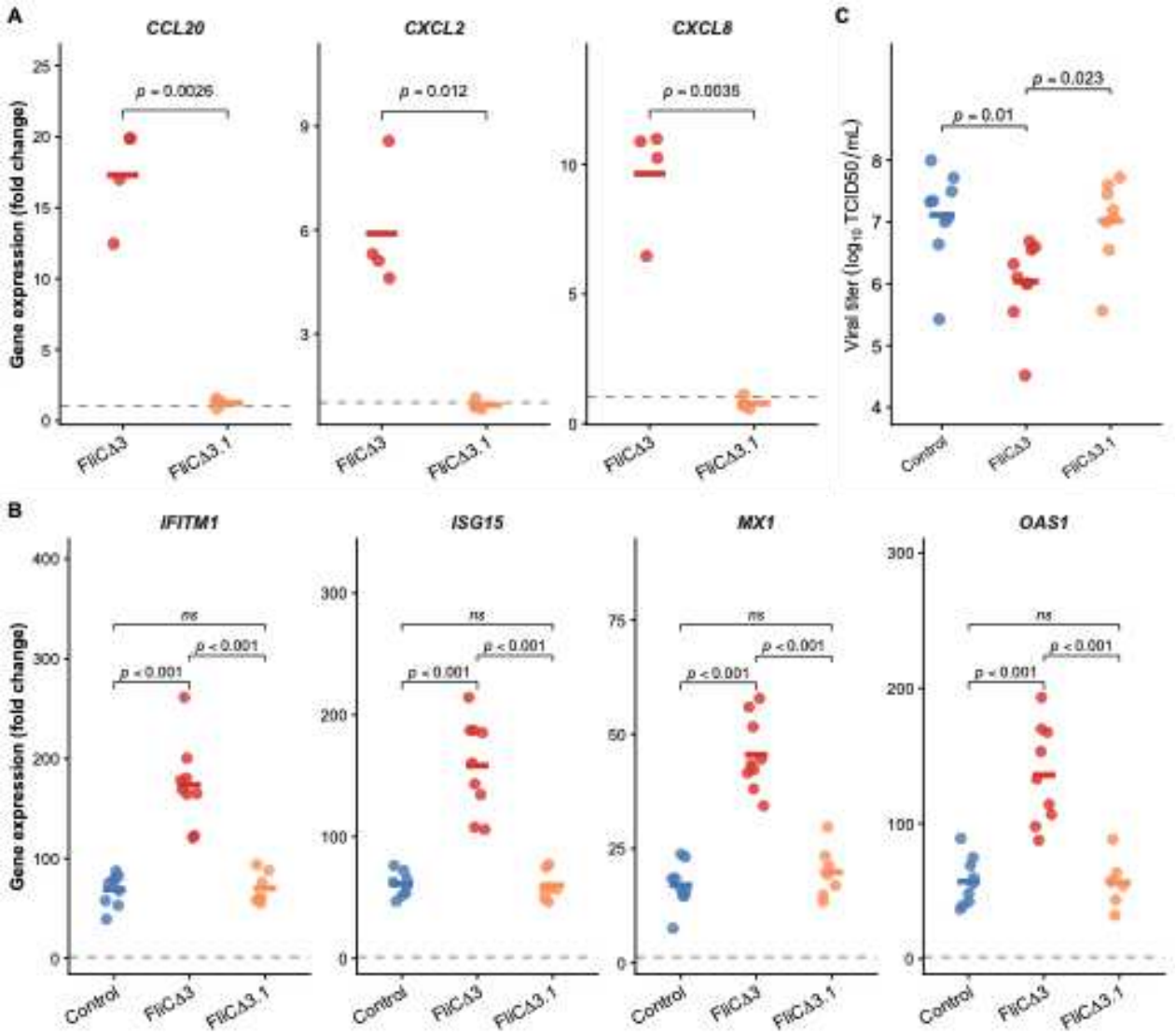


Figure 3. The immunomodulatory and antiviral effects of flagellin are TLR5-dependent. T3 cells were infected with SIAV H3N2 and treated with bioactive flagellin (FliC$_{\Delta 3}$), TLR5-non-signaling mutant (FliC$_{\Delta 3.1}$), or left untreated (Control) for 4 hours. (A) Chemokine expression in infected cells treated with FliC$_{\Delta 3}$ or FliC$_{\Delta 3.1}$. p values from unpaired two-sided Student's t-test (n = 4). (B) ISG expression in SIAV-infected cells treated with FliC$_{\Delta 3}$, FliC$_{\Delta 3.1}$, or left untreated (Control). Brackets indicate pairwise comparisons from one-way ANOVA followed by Tukey HSD post-hoc test (n = 7–9); ns, not significant. (C) Viral titers at 48 hpi determined by TCID50 assay on MDCK cells. p values from one-way ANOVA followed by Tukey HSD (n = 8–9). Each dot represents an individual biological replicate; horizontal bars indicate the mean. Dashed grey line indicates the mean expression level of non-infected untreated controls (A, B). Data in (A) and (B) are expressed as fold change relative to non-infected untreated cells.

FLAMOD effect on the antiviral response is predominantly dependent on JAK signaling

Most ISGs are regulated by IFN-I (IFNα/β) via the JAK/STAT pathway, with emerging evidence indicating that NF-κB can also regulate a subset of ISGs[28]. To dissect their relative contributions to FLAMOD-mediated antiviral responses, we used chemical inhibitors targeting NF-κB (BAY 11-7082, an IKK inhibitor) and JAK/STAT signaling (JAK inhibitor I). One hour pre-treatment of T3 cells with JAK inhibitor I completely abolished FLAMOD-induced ISG expression (*IFITM1*, *ISG15* and *OAS1*) in SIAV-infected cells at 48 hpi (Figure 4A). Moreover, FLAMOD antiviral effect was entirely lost in the presence of the JAK inhibitor (Figure 4B). In contrast, NF-κB inhibition with BAY 11-7082 reduced the expression of pro-inflammatory cytokines (CCL20) and selected ISGs (OAS1) at 48 hpi (Supplementary Figure 2) but did not impair FLAMOD antiviral activity (Supplementary Figure 2). Taken together, these data indicate that FLAMOD's antiviral activity against SIAV H3N2 is predominantly mediated through JAK/STAT signaling rather than NF-κB.

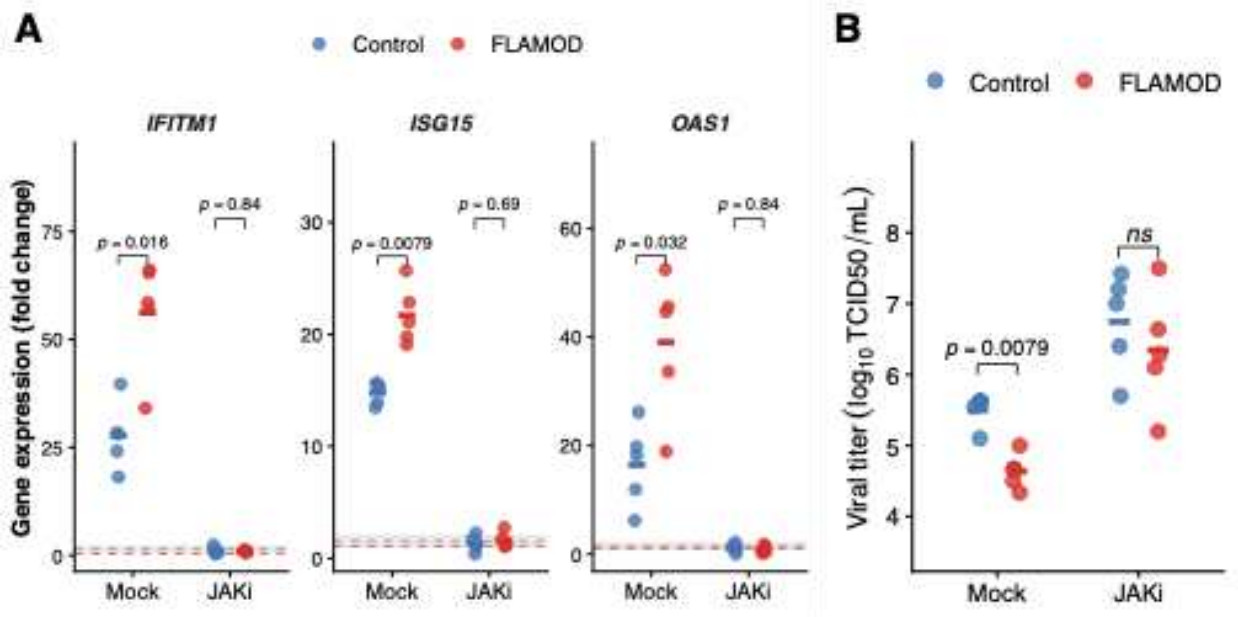


Figure 4. FLAMOD-mediated antiviral response is dependent on JAK/STAT signaling. T3 cells were pre-treated with JAK inhibitor I (JAKi) or vehicle (Mock) for 1 hour, infected with SIAV H3N2, and treated with FLAMOD or left untreated (Control) for 48 hours. (A) ISG expression measured by RT-qPCR. Data are expressed as fold change relative to non-infected, untreated controls (grey dashed line). Non-infected, FLAMOD-treated samples are represented as a red dashed line. Shaded areas represent the standard error of the mean for the respective non-infected baselines. (B) Viral titers at 48 hpi determined by $TCID_{50}$ assay on MDCK cells. Each dot represents an individual biological replicate (n = 5); horizontal bars indicate the mean. p values were calculated using two-sided Wilcoxon rank-sum tests comparing FLAMOD-treated and untreated groups within each inhibitor condition; ns, not significant.

FLAMOD effect on the antiviral response requires IFN-I signaling

To confirm the requirement for IFN-I signaling, we generated an *IFNAR1*-knockout (*IFNAR1*-KO) T3 cell line using CRISPR/Cas9 genome editing. Sanger sequencing confirmed disruptive indels in 91% of alleles (Supplementary Figure 3). Confocal microscopy imaging of edited cells showed an almost complete absence of IFNAR1, with just 24% of *IFNAR1*-KO cells retaining residual IFNAR1 signal (Figure 5A and

Supplementary Figure 3). Stimulation with 10 IU/mL IFN-α for 30 min induced robust nuclear translocation of STAT2 in NTC cells. In contrast, STAT2 remained cytoplasmic in *IFNAR1*-KO cells, confirming their inability to respond to IFN-I due to loss of receptor signaling (Figure 5B).

To determine the contribution of IFN-I signaling to FLAMOD-mediated antiviral responses, non-targeting control (NTC) and *IFNAR1*-KO cells were infected with SIAV H3N2 (MOI 0.1) for 1 hour, treated with 100 ng/mL of FLAMOD or left untreated, and sampled at 8, 24, and 48 hpi. The expression of ISGs (*ISG15*, *MX1*, *OAS1*) increased progressively, peaking at 48 hpi in NTC cells. As observed previously, FLAMOD treatment further amplified ISG induction (Figure 5C). ISG induction was profoundly reduced in *IFNAR1*-KO cells, with *ISG15* induction being almost completely abrogated (Figure 5C). FLAMOD induced early and sustained expression of *CCL20* and *CXCL8* (Figure 5D). Notably, *CCL20* expression was significantly reduced in IFNAR1-KO cells relative to NTC cells ($p < 0.005$, Figure 5D). In contrast, *CXCL8* expression did not differ significantly between *IFNAR1*-KO and NTC cells (Figure 5D).

Finally, FLAMOD significantly reduced viral titers in NTC cells, but this antiviral effect was entirely lost in *IFNAR1*-KO cells (Figure 5E). Together, these findings demonstrate that functional IFN-I signaling through the IFNAR–JAK–STAT pathway is essential for mediating the antiviral effect of FLAMOD *in vitro*.

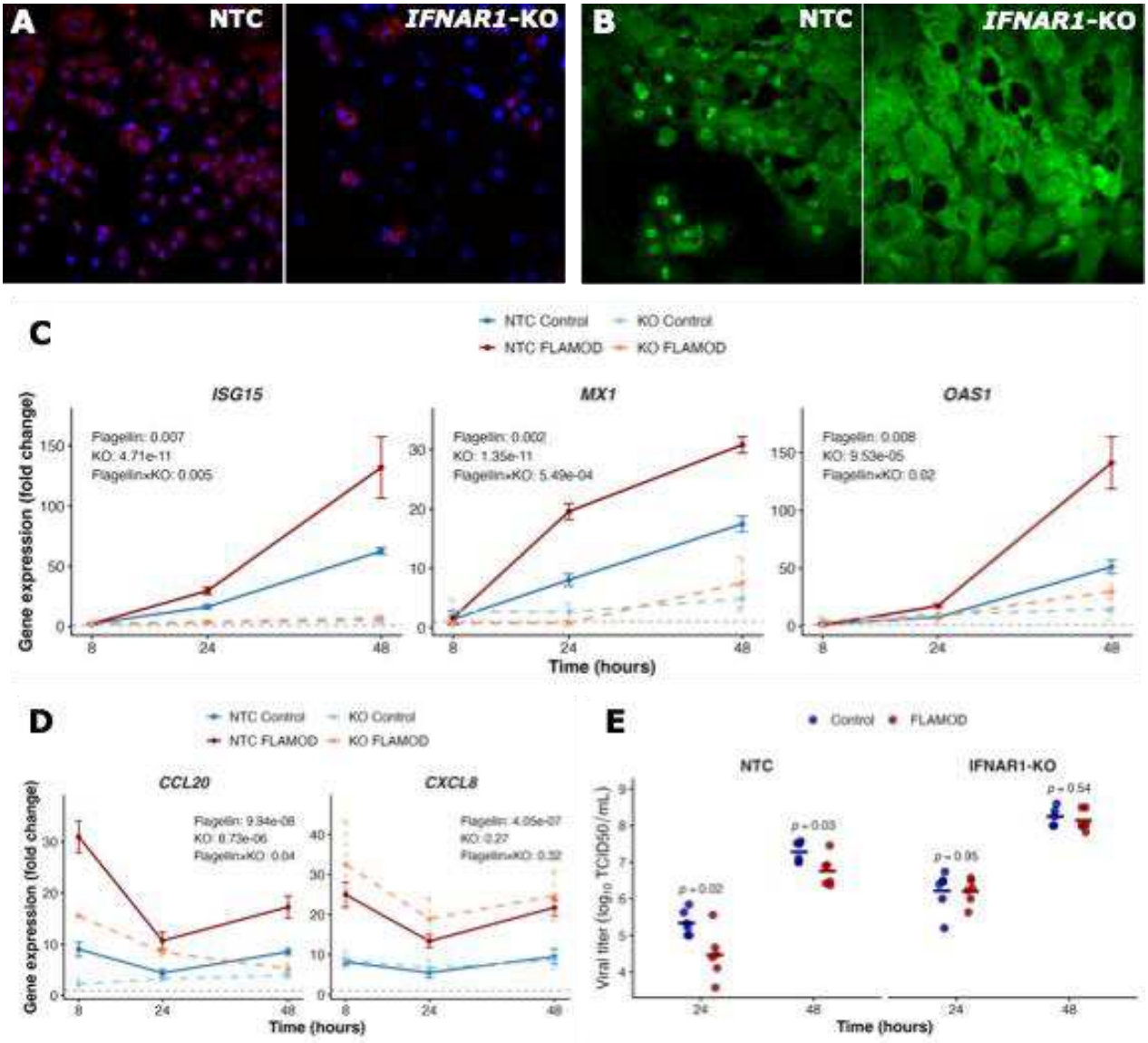


Figure 5. Type I interferon signaling is required for FLAMOD-mediated antiviral activity. (A) Immunofluorescence staining of IFNAR1 in NTC and *IFNAR1*-KO T3 cells. Red, IFNAR1; blue, DAPI. (B) STAT2 nuclear translocation in NTC and *IFNAR1*-KO cells after stimulation with recombinant type I interferon (10 U/mL, 30 min). Green, STAT2. (C) ISG expression (ISG15, MX1, OAS1) in SIAV H3N2-infected NTC and *IFNAR1*-KO cells treated with FLAMOD (100 ng/mL) or vehicle control. (D) Chemokine expression (*CCL20*, *CXCL8*) in the same experimental conditions. Data in (C) and (D) are expressed as mean fold change ± SEM relative to non-infected untreated controls (dashed grey line) (n = 3-6 per group per time point). p values from three-way ANOVA (Flagellin × Time × KO) indicate the main effect of FLAMOD treatment, genotype (KO), and their interaction (Flagellin × KO). Solid lines, NTC; dashed lines, *IFNAR1*-KO. (E) Viral titers at 24 and 48 hpi determined by $TCID_{50}$ assay on MDCK cells. Each dot represents an individual biological replicate (n = 5-6); horizontal bars indicate the mean. p values from unpaired two-sided Student's t-test comparing FLAMOD-treated and untreated groups within each genotype and time point.

FLAMOD enhances cellular sensitivity to interferon, leading to an increased expression of ISG genes.

Our results showed that FLAMOD amplifies ISGs expression only during infection (Figure 1A). To elucidate whether FLAMOD sensitizes porcine airway epithelial cells to IFN-I, we quantified the nuclear translocation of STAT2, a component of the ISGF3 complex[29,30]. T3 cells were treated with increasing concentrations of porcine IFN-α (0, 0.1, 1, 2.5, 5, and 10 IU/mL), either alone or in combination with 100 ng/mL of FLAMOD. STAT2 nuclear translocation was assessed at 15, 30, and 60 minutes post-stimulation.

FLAMOD alone did not induce STAT2 nuclear translocation, consistent with its inability to activate the JAK-STAT pathway. In contrast, IFN-α alone induced a dose-dependent STAT2 translocation. Kinetic analysis showed distinct patterns depending on IFN-α concentration. STAT2 translocation was transient at 2.5 IU/mL (with a peak at 30 min) but rapid and sustained at 5–10 IU/mL (Figure 6A).

Co-treatment with FLAMOD and IFN-α shifted this response toward lower IFN-α concentrations, with STAT2 translocation detectable at 1 IU/mL IFN-α by 15 minutes and sustained thereafter (Figure 6A). The proportion of cells exhibiting nuclear STAT2 was significantly higher in the FLAMOD + IFN-α condition, even at low IFN-α doses (Supplementary Figure 4).

We calculated the area under the curve (AUC) and confirmed a significant increase in STAT2 nuclear translocation when FLAMOD was combined with low IFN-α concentrations (1 and 2.5 IU/mL) (Supplementary Figure 4). At the highest IFN-α doses, no differences were observed between the two conditions. Log-logistic fitting showed that both conditions exhibited ultrasensitive responses, with Hill coefficients of 2.43 (IFN-α alone) and 2.16 (FLAMOD + IFN-α) but a 12-fold reduction in EC_{50} in the presence of FLAMOD (EC_{50} = 0.21 IU/mL) compared to IFN-α alone (EC_{50} = 2.47 IU/mL) (Figure 6B).

This sensitization extended to gene expression. ISG (*IFITM1*, *MX1* and *OAS1*) expression at 4 hours post-treatment increased in a dose-dependent manner, mirroring the trend observed for STAT2 activation (Figure 6C). However, ISG expression did not plateau at the highest IFN-α concentration tested (10 UI/mL) (Figure 6C). Importantly, at low IFN-α doses (1 UI/mL), cotreatment with FLAMOD already induced detectable *IFITM1* and *OAS1* expression, while IFN-α alone remained near basal levels (Figure 6C).

Altogether, FLAMOD strengthens IFN-I signaling in porcine AECs, promoting rapid antiviral gene activation.

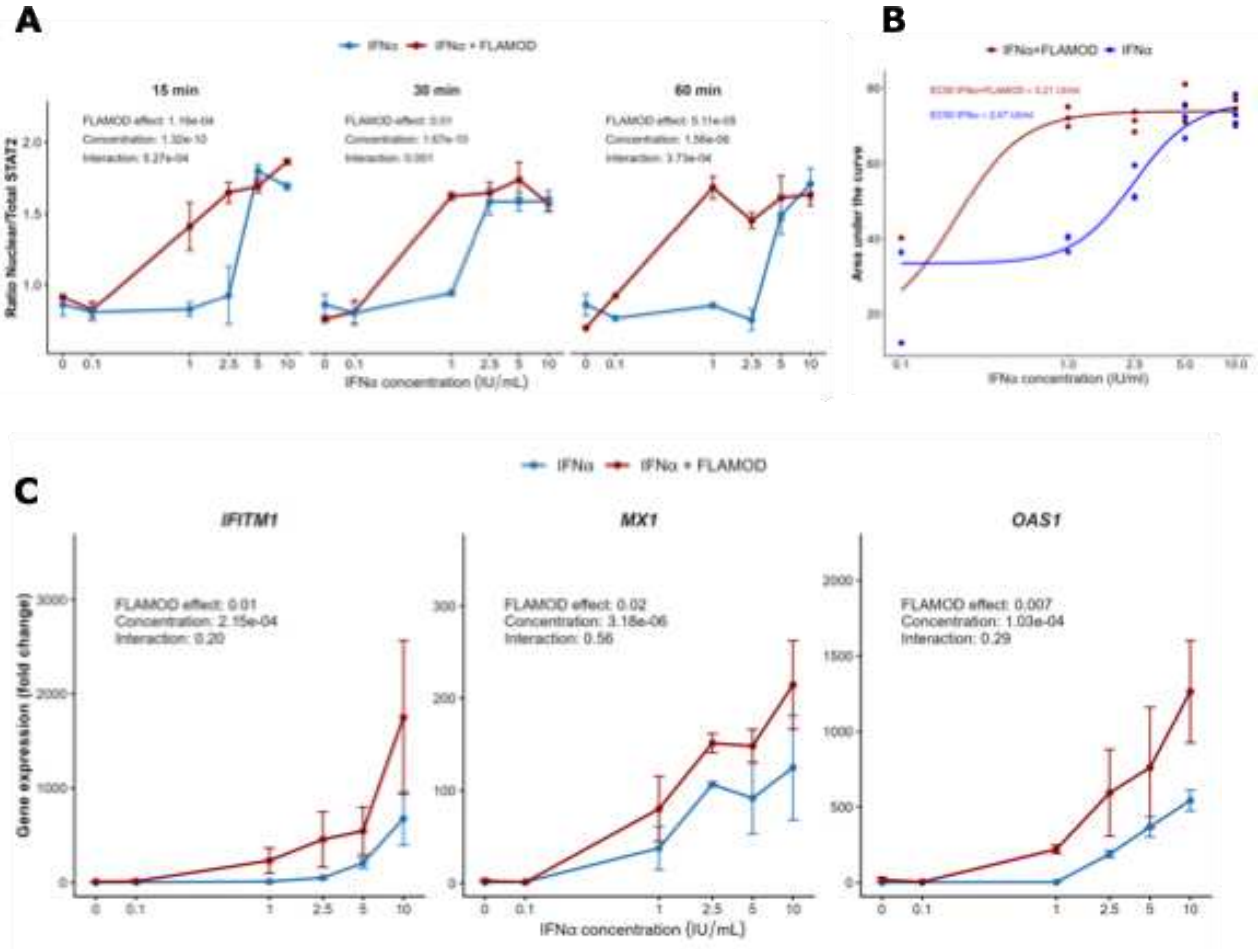


Figure 6. FLAMOD enhances T3 cells sensitivity to interferon-α. T3 cells were treated with FLAMOD (100 ng/ml) or vehicle control and different concentrations (0-10 IU/mL) of interferon-α (IFNα) for 15, 30 or 60 minutes (A-B) or 4 hours (C). (A) Dose-response evaluation of STAT2 nuclear translocation (n= 3). (B) Log-logistic model for the area under the curve of the ratio nuclear/total STAT2 for each dose of IFNα.The half-maximal effective concentration (EC50) values are displayed for cells stimulated with IFNα or IFNα and FLAMOD. (C) Dose responses for the expression off *IFITM1*, *MX1* and *OAS1* (n = 3). Data in (A) are expressed as mean nuclear/total STAT2 ratio ± SEM; data in (C) are expressed as mean fold change ± SEM relative to non-treated controls. P values from two-way ANOVA indicate the main effect of FLAMOD treatment, IFNα concentration and their interaction.

MyD88, but not TRAF6, is required for the effect of FLAMOD on IFN-I signaling

To dissect how TLR5 signaling interacts with the IFN-I pathway, we generated TRAF6-knockout (*TRAF6*-KO) and MyD88-knockout (*MYD88*-KO) T3 cell lines by CRISPR/Cas9 genome editing (sgRNAs used in the study are shown in Table S1). Sanger sequencing revealed disruptive indels in approximately 67% of *TRAF6* (Supplementary Figure 5) and 63% of *MYD88* (Supplementary Figure 6) alleles.

Cells were stimulated for 4h with either IFN-α (10 UI/mL), IFN-α (10 UI/mL) plus FLAMOD (100 ng/mL) or the buffer. IFN-α alone induced ISGS (*MX1*, *OAS1*, *IFITM1*) to comparable levels across NTC, *TRAF6*-KO and *MYD88*-KO, confirming intact baseline IFN responsiveness (Figure 7A and 7B). FLAMOD co-treatment enhanced ISG expression in

control cells. This enhancement was preserved in *TRAF6*-KO cells, with no significant difference between genotypes (Figure 7A). In contrast, MyD88 deletion abolished the FLAMOD-mediated ISG enhancement for *MX1* and *IFITM1*, while *OAS1* showed a similar trend ($p = 0.12$). In contrast, FLAMOD-induced *CCL20* and *CXCL8* expression was lost in both *TRAF6*-KO and *MYD88*-KO. Together, these results support the existence of two distinct signaling branches: FLAMOD potentiates IFNα-driven ISG expression through MyD88 independently of TRAF6, while FLAMOD-induced pro-inflammatory gene expression requires both MYD88 and TRAF6, consistent with canonical NF-κB activation.

To investigate whether MYD88 physically associates with the JAK–STAT pathway, we performed co-immunoprecipitation assays in T3 cells stimulated for 30 min with FLAMOD alone, IFN-α alone, FLAMOD plus IFN-α, or left unstimulated. JAK1 co-precipitated with endogenous MyD88 exclusively under combined FLAMOD and IFN-α stimulation; no interaction was detected with either agonist alone or in unstimulated cells (Figure 7C). These results indicate that concurrent activation of TLR5 and IFNAR promotes the formation of a MyD88–JAK1 complex, providing a mechanistic basis for the FLAMOD-mediated amplification of type I IFN signaling.

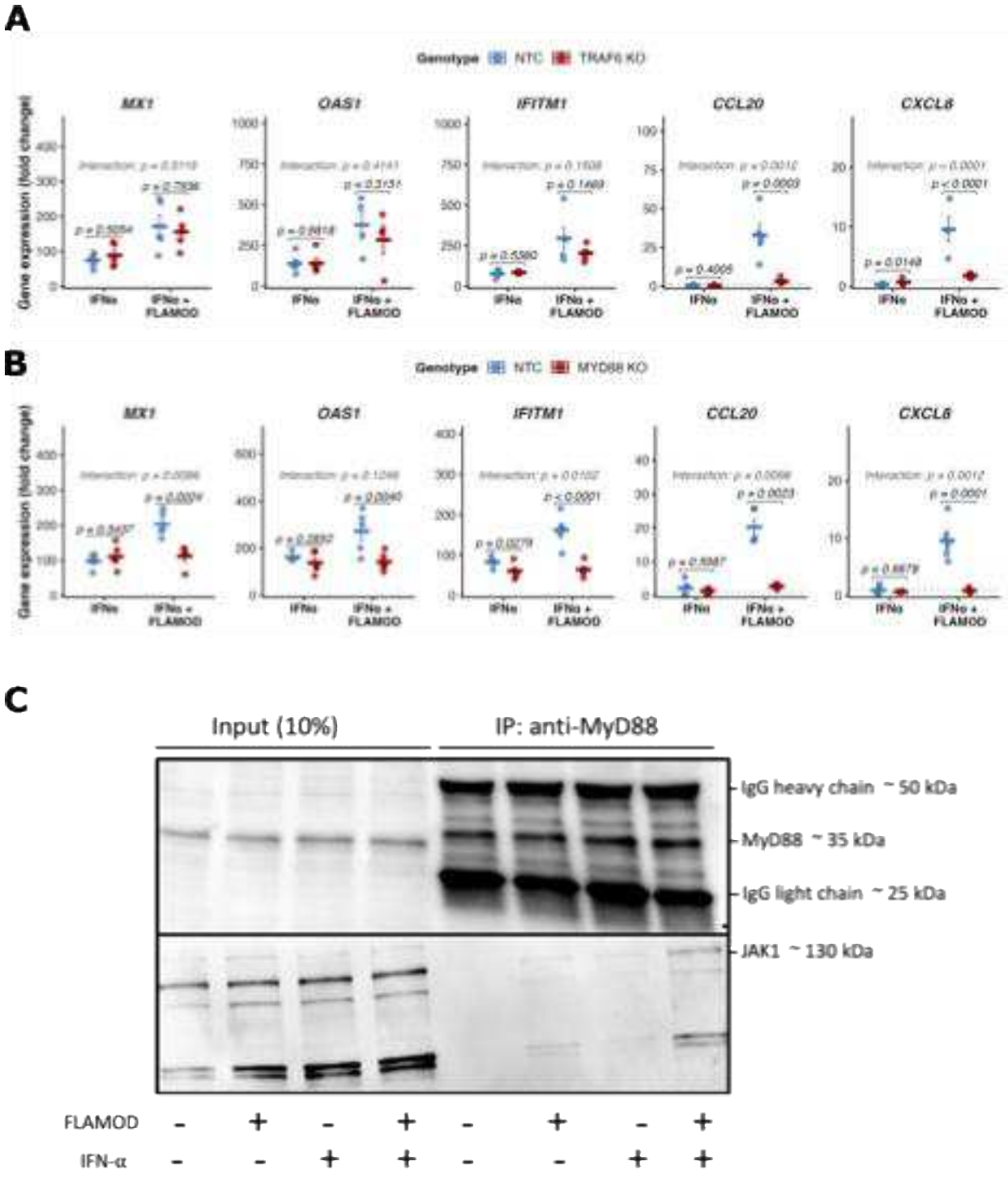


Figure 7. MYD88, but not TRAF6, is required for FLAMOD-mediated amplification of type I interferon signaling. (A, B) Relative gene expression (fold change over mock) of ISGs (MX1, OAS1, IFITM1) and pro-inflammatory cytokines (CCL20, CXCL8) in NTC versus TRAF6 KO (A) or MYD88 KO (B) cells treated with IFNα or IFNα + FLAMOD. Crossbars indicate group means; error bars ± SEM; dashed line = mock baseline. Data were analyzed by linear mixed-effects models on ΔΔCt (Treatment × Genotype + (1|Day)). Interaction p-values report the Treatment × Genotype term. *p* values report simple effects of Genotype within each Treatment (Holm-adjusted) (n =5). TRAF6 and MYD88 knockdown efficiencies are shown in Supplementary Figures 5 and 6. (C) T3 cells were stimulated for 30 min with FLAMOD, IFNα, FLAMOD + IFNα, or left unstimulated. Proteins

were immunoprecipitated using an anti-MYD88 antibody and the result was analyzed by western blot by probing membranes with anti-MYD88 and subsequently reprobing with anti-JAK1. Representative western blot corresponding to the immunoprecipitates are shown on the right whereas western blots on input samples (10% of lysate) are shown on the left. Bands at 50 kDa and 25 kDa correspond to IgG heavy and light chains. JAK1 co-precipitates with MYD88 exclusively upon co-stimulation (n = 3).

FLAMOD decreases clinical symptoms and systemic inflammation in SIAV-infected pigs

To evaluate the effect of FLAMOD *in vivo*, pigs were infected with SIAV $H1_{av}N2$ and treated with FLAMOD or vehicle one-hour post-inoculation. Clinical monitoring revealed distinct disease trajectories between treatment groups throughout the 72h observation period (Figure 8A). Clinical signs, including increased respiratory frequency, irregular breathing, cough, lethargy, and reduced mobility, were observed exclusively in $H1_{av}N2$-infected animals.

FLAMOD significantly reduced cumulative clinical scores (Figure 8B). This protective effect was most pronounced during the acute disease phase, with clinical signs in FLAMOD-treated pigs largely restricted to 6 hpi. Half of the FLAMOD-treated animals (3/6, 50%) remained completely asymptomatic throughout the trial, in contrast to symptom development in all the animals from the control group (6/6, 100%), in which animals were administered the NaPi buffer.

Likewise, FLAMOD also attenuated systemic inflammation. Serum C-reactive protein (CRP) concentrations, were significantly reduced in FLAMOD-treated animals compared to animals from the control group (Figure 8C).

Finally, we assessed whether a single FLAMOD administration could reduce pulmonary viral titers *in vivo*. We observed that FLAMOD-treated pigs exhibited a non-significant downward trend in viral loads (2.1-fold, $p = 0.16$) compared to NaPi-treated (Figure 8D). These results suggest that FLAMOD can modulate the inflammatory response to SIAV and may mitigate SIAV-associated pathology.

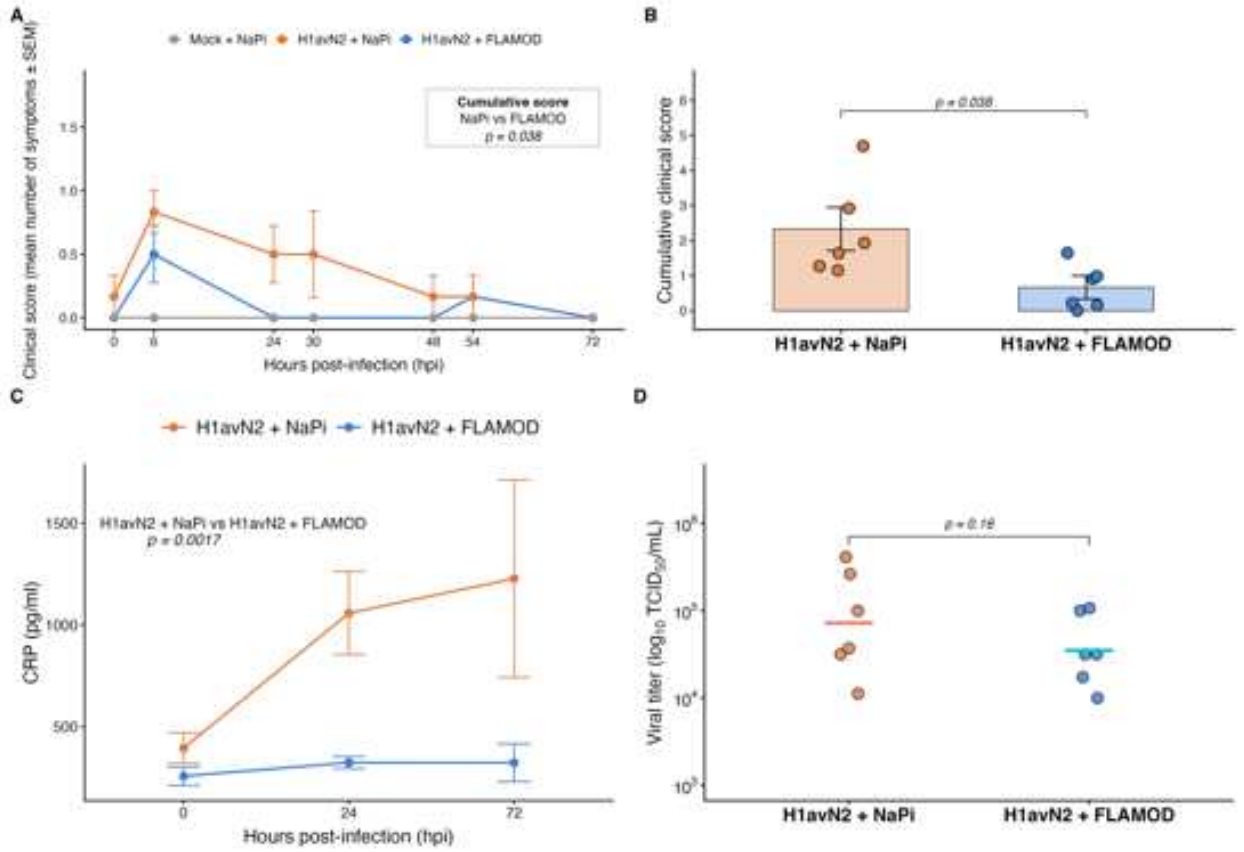


Figure 8. FLAMOD decreases clinical symptoms and systemic inflammation in SIAV-infected pigs. (A-B) Clinical score represents the sum of distinct clinical manifestations per animal per timepoint. (A) Clinical score time course showing mean number of symptoms ± SEM over 72 hpi (hpi) for mock-infected controls, $H1_{av}N2$-infected pigs treated with the buffer (NaPi), and $H1_{av}N2$-infected pigs treated with FLAMOD. Clinical signs included increased respiratory frequency, irregular breathing, cough, lethargy, and reduced mobility. Cumulative clinical scores (sum of all symptoms across all timepoints per animal) comparing $H1_{av}N2$-infected pigs treated with NaPi buffer or FLAMOD. Each dot represents an individual replicate (n = 6). *p* values were determined using Student's t-test. (C) Serum C-reactive protein (CRP) concentrations over time in $H1_{av}N2$-infected pigs treated with NaPi buffer (orange) or FLAMOD (blue). Data points represent means ± SEM at 0, 24, and 72 hpi. CRP was analyzed by linear mixed-effects model on log-transformed values with Treatment, Day, and their interaction as fixed effects and Pig as a random intercept (lmerTest). (D) Viral titers in the pig lungs (right cranial lobe) at 72 hpi determined by $TCID_{50}$ assay on MDCK cells, expressed as log_{10} $TCID_{50}$ per gram of tissue. Each dot represents an individual biological replicate (n = 6); horizontal bars indicate the mean. Statistical analysis was a one-sided Student's t-test based on the *a priori* hypothesis that FLAMOD would reduce viral replication as observed i*n vitro*.

FLAMOD treatment increases the expression of ISGs in $H1_{av}N2$-infected pigs

To assess how FLAMOD modulates the host transcriptional response to SIAV, we performed single-nucleus RNA sequencing (snRNA-seq) on lung tissue collected at 3 days post-inoculation from control pigs (n = 3), $H1_{av}N2$-NaPi animals (n = 6) and $H1_{av}N2$-FLAMOD animals (n = 6). After quality control, a total of 135349 nuclei were integrated

across all samples. Iterative clustering and marker-based annotation resolved 30 cell populations spanning the porcine lung cellular landscape (Figure 9A and Supplementary Figure 7). $H1_{av}N2$ infection reduced B cell and club cell proportions, and expanded cDC1s, monocyte-derived macrophages, pDCs, plasma cells, and proliferating lymphocytes, consistent with an active innate and early adaptive immune response. Importantly, composition did not differ between $H1_{av}N2$-NaPi and $H1_{av}N2$-FLAMOD animals (Supplementary Figure 8), indicating that FLAMOD does not substantially alter lungs cellular composition at this stage.

Among cells with detectable viral RNA, this distribution of the percentage of total RNA reads was bimodal on a log-scale (Supplementary Figure 9). A two-component Gaussian mixture model defined four infection states: control, bystander, low, and high (Figure 9B). High-load cells were predominantly of respiratory epithelial origin. Surprisingly, some cell types (basal, lymphatic endothelial and pDC), showed a significant increase in the number of viral transcripts in FLAMOD treated animals (Supplementary Figure 10).

Per-cell type I and type II ISGs module scores were significantly elevated in cells from infected animals relative to uninfected controls, including in bystander cells that contained no detectable viral RNA (Figure 9C). This indicates that tissue-level inflammation via paracrine interferon signaling rather than per cell viral burden, governs ISG magnitude.

We next performed differential expression analysis between FLAMOD- and NaPi- treated animals for each cell type and infection state combination, followed by gene-set enrichment analysis (GSEA) of type I and type II ISGs (Supplementary Figure 11 and Supplementary Figure 12, respectively). FLAMOD significantly induced ISG expression in most cell types (Figure 9D), with the strongest effects observed in NK cells, smooth muscle, B cells, basal cells and naïve T cells. In contrast, multiciliated cells and activated IMs showed attenuated ISG responses. FLAMOD-mediated ISG induction was reduced in cell presenting high viral loads (Figure 9D). A donor-level random-effects meta-analysis of ISG module scores for each infection state confirmed the increase in type I and type II ISG scores in most bystander and low viral load cell types (Supplementary Figures 13 and 14), with no detectable heterogeneity across cell types in the magnitude of the effect ($I^2 = 0\%$). In high viral load cells, the pooled effect was attenuated and no longer significant. Together, these findings indicate that FLAMOD broadly sensitizes IFN signaling across the lung cellular landscape, with the strongest effect in bystander cells.

At the gene level, FLAMOD upregulated ISGs predominantly in bystander cells, with the largest number of differentially expressed ISGs in immune cell types (Figure 9E and Supplementary Figure 15). *IFITM3,* an antiviral ISG with anti-influenza activity[31], was the most consistently induced ISG. Other classical ISGs, including *OAS2, MX2, EIF2AK2, IFI44, IFIH1,* were upregulated in various cell types. Importantly IFN-I module scores did not differ across lung cell types between treatments and did not correlate with the ISG response (Supplementary Figure 16). These results indicate that the enhanced ISG program in FLAMOD-treated animals reflects increased cellular responsiveness IFN signaling rather than elevated IFN production at the time of sampling.

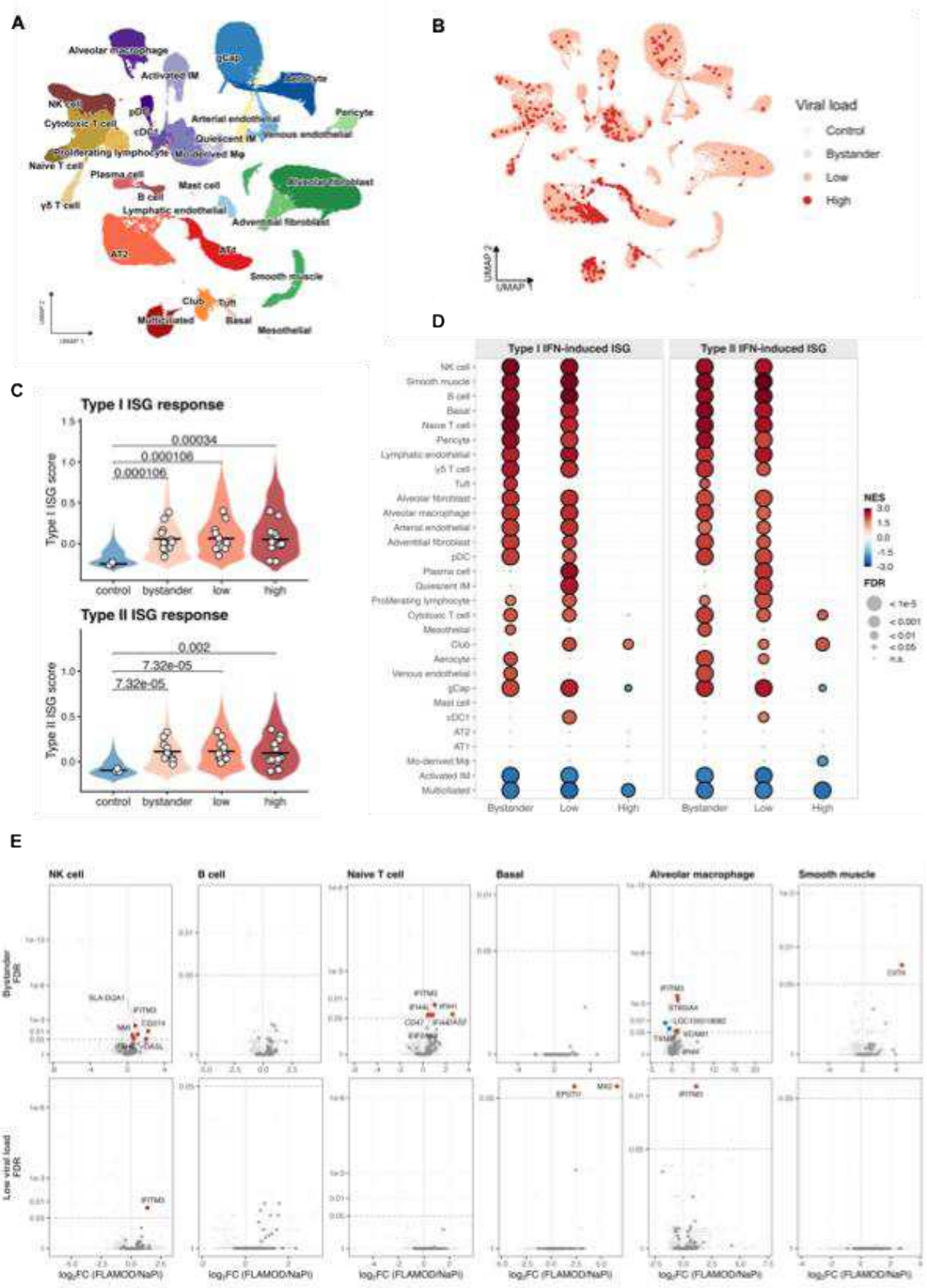


Figure 9. FLAMOD increases ISG expression in H1$_{av}$N2 infected pigs. (A) UMAP visualization of 30 cell types annotated across all samples (18260 cells from the control group, 48071 cells from H1avN2-NaPi, and 69019 cells from H1avN2-FLAMOD animals).

(B) UMAP projection colored by viral load category: control (no infection), bystander (no detectable viral reads in infected animals), low, and high viral load. (C) Type I (top) and Type II (bottom) ISG module scores across viral load categories. Violins show the distribution of single-cell scores; overlaid white dots represent per-animal pseudobulk means (n ≥ 5 cells per animal per category). Horizontal black bars indicate group means. P-values are from pairwise t-tests on pseudobulk values with Benjamini–Hochberg correction; only significant comparisons are shown. (D) Pseudobulk gene set enrichment analysis (GSEA) of Hallmark type I and type II IFN-induced gene sets across lung cell types and infection states. For each cell type × infection state, gene-level differential expression between FLAMOD- and NaPi-treated animals was performed by DESeq2 on per-pig pseudobulk counts, and genes were ranked by the Wald statistic for input to fgsea. Bubble color indicates the normalized enrichment score (NES); bubble size indicates the Benjamini-Hochberg-adjusted enrichment FDR. Cell types are ordered by mean NES across infection states. (E) Volcano plots of differentially expressed ISGs between FLAMOD and NaPi in bystander and cells with low viral loads in selected cell types. Red and blue dots indicate genes significantly upregulated and downregulated in FLAMOD-treated animals, respectively (FDR < 0.05). Dark grey indicates non-significant ISGs. Light grey indicates non-ISG genes. Gene labels are shown for significant genes only. Statistical significance was assessed by DESeq2 Wald test on pseudobulk counts (FLAMOD vs NaPi); FDR is Benjamini-Hochberg-adjusted across all genes per cell type.

DISCUSSION

Rational design of TLR-based therapeutic interventions requires a good understanding of how TLR signaling intersects with the IFN response. Here, using SIAV-infected porcine bronchial epithelial and an *in vivo* pig model, we identify a previously unrecognized interaction between TLR5 and the IFN-I axis. We demonstrate that TLR5 activation by FLAMOD sensitizes lung cells to IFN-I signaling, enhancing ISG expression in both infected and bystander cells and potentially reducing SIAV viral titers.

The antiviral potential of TLR ligands is well-documented. TLRs can induce type I IFN induction via IRF3/7 signaling[32,33]. Flagellin administration has shown protective effects in murine models of viral infections, including rotavirus[34], CMV[35] and influenza A virus (IAV) infections[17,19]. However, the underlying mechanisms remain debated. Although flagellin can induce antiviral ISGs in mouse lungs[19], studies in IFN-receptor-deficient mice suggest its protection may occur independently of IFN signaling, relying on recruitment of NK cells[35], DCs[34] and neutrophils[17]. The cell-intrinsic basis of flagellin's antiviral activity, particularly in airway epithelial cells, has remained unclear.

In contrast to previous studies conducted in murine models, we found that FLAMOD-induced ISG expression correlated with reduced viral titers *in vitro,* and this antiviral effect was abolished when ISG expression was disrupted. *In vivo*, FLAMOD administration increased ISGs expression across various lung cell populations in SIAV-infected pigs. Although single-nucleus RNA sequencing (snRNA-seq) revealed stable or slightly increased viral RNA in some cell types, lung viral titers trended downward in FLAMOD-treated animals. This apparent discrepancy aligns with the "abortive" nature of the influenza infection cycle, in which viral transcription is often uncoupled from the production of infectious progeny[36]. Recent mapping of the IAV infection cycle suggests that many cells reach high levels of viral mRNA but fail to produce infectious virions due to intracellular bottlenecks in genome replication or assembly[37,38]. Our findings suggest that

FLAMOD-induced ISGs may primarily interfere with the late stages of the viral life cycle. Thus, higher viral RNA detected by snRNA-seq could reflect trapped or non-productive transcripts in cells that are more effectively restricting the virus. Larger cohorts and optimized dosing will be required to fully define the antiviral efficacy of TLR5 activation *in vivo*.

A central question is how FLAMOD drives ISG upregulation. Since pigs lack a functional NAIP/NLRC4 inflammasome[39], intracellular flagellin sensing can be excluded. We confirmed TLR5-dependence using a mutated flagellin unable to bind TLR5 that failed to induce ISGs. Murine studies propose that flagellin induces type I IFN, driving ISG expression via canonical JAK-STAT signaling[21,40]. Our data point to a distinct mechanism in pigs. FLAMOD-treated SIAV-infected cells showed only a slight trend toward increased IFNβ. Instead, co-stimulation with FLAMOD and IFN-α markedly increased nuclear translocation of STAT2 and enhanced ISG expression, even at concentrations of IFN-α that were insufficient to trigger ISG expression. Therefore, FLAMOD sensitizes cells to IFN signaling rather than inducing it. snRNA-seq data showed that this sensitization occurred regardless of infection status, indicating that FLAMOD acts directly on the IFN-I signaling axis, potentiating both autocrine and paracrine IFN responses across the epithelial cell population.

This raises the question of where TLR5 signaling intersects with the JAK-STAT pathway. Upon flagellin binding, TLR5 recruits MyD88 forming the myddosome, engaging IRAK4, IRAK1, TRAF6, and ultimately NF-κB[20,41]. However, the rapid enhancement of STAT2 nuclear translocation (within 15 minutes) argues against an NF-κB-dependent transcriptional mechanism. Crosstalk between TLR signaling components and JAK-STAT has been reported before. TRAF6 can negatively regulate JAK-STAT signaling by promoting ubiquitination of STAT3[42], while MyD88 can form complexes with JAK1 and STAT1 in macrophages[43]. This complex formation was associated with induction of SOCS-1 and the suppression of cytokine signaling rather than with enhanced interferon responsiveness[43]. Our data support a functionally distinct MyD88-JAK1 interaction. Neither IKK inhibition nor TRAF6 knockout affected the synergistic ISG induction by FLAMOD and IFN-α, whereas MyD88 deletion abolished it, placing the branch point at MyD88 upstream of the TRAF6-NF-κB axis. Consistent with this, co-immunoprecipitation revealed an interaction between MyD88 and JAK1 specifically under combined TLR5 and IFNAR stimulation.

Altogether, our data support a model in which TLR5 activation by FLAMOD primes the JAK-STAT signaling machinery through a MyD88–JAK1 interaction, lowering the threshold for IFN-I responsiveness. When an IAV-infected cell releases IFN, neighboring and infected cells previously exposed to FLAMOD mount a stronger and faster ISG response than they would to IFN alone. Because this mechanism acts on the IFN signaling pathway itself rather than on any virus-specific component, it is likely not restricted to influenza and may apply to a broad range of viruses restricted by IFN-I. These findings obtained in porcine airway epithelial cells and validated *in vivo* are particularly relevant given the pig's dual role as a major livestock species and a key reservoir for IAV reassortment, as well as its value as a model for human respiratory disease.

MATERIALS AND METHODS

Cell line, reagents and flagellin production

The T3 cell line was generated from primary porcine bronchial epithelial cells and maintained in supplemented huAEC medium (Inscreenex) as described elsewhere[12].

Recombinant porcine IFN-α was purchased from PBL Assay Science (USA). Working concentrations of 10 μM JAK Inhibitor I (Millipore) and 5 μM BAY 11-7082 (Sigma-Aldrich) were applied to T3 cells throughout the experiment. Antibodies are listed in Supplementary Methods. Cytotoxicity was evaluated by CytoTox-Glo™ Cytotoxicity Assay (Promega).

FLAMOD (recombinant flagellin $FliC_{\Delta 174\text{-}400}$) derived from *Salmonella enterica* serovar Typhimurium FliC [17,25] and was produced as described previously[12,17,44]. The endotoxin content was < 14 endotoxin units per mg of FLAMOD, as determined by the Limulus amebocyte lysate assay. The TLR5-inactive mutated flagellin variant, $FliC_{\Delta 174–400/89–96*/6H}$, ($FliC_{\Delta 3.1}$), was generated by replacing the TLR5-binding epitope (residues 89–96, QRVRELAV) of the active $FliC_{\Delta 174–400/6H}$ variant ($FliC_{\Delta 3}$) with the corresponding sequence from *Helicobacter pylori*[45–47].

Viruses and infection of T3 cells

The H3N2-Bissendorf03 strain (A/Swine/Bissendorf/IDT1864/2003) and the $H1_{av}N2$ strain (A/Swine/35-200154/2020; HA-1C.2.4) were propagated in Madin-Darby canine kidney (MDCK) cells at a multiplicity of infection (MOI) of 0.001. T3 cells were seeded in collagen-coated sterile 24-well plates at a density of 2×10^5 cells per well and infected at an MOI of 0.1 for 1h, washed and treated or not with 100 ng/mL of FLAMOD, $FliC_{\Delta 3}$ or $FliC_{\Delta 3.1}$ as indicated. Viral titers were determined on MDCK cells by $TCID_{50}$ (Reed-Muench method). *In vivo* titers in the lungs were calculated using a homogenate from the right cranial lobe.

Immunofluorescence

T3 cells were fixed, permeabilized blocked and stained with the corresponding primary antibodies overnight at 4°C, followed by 1h incubation with the appropriate secondary antibodies. Nuclei were stained with DAPI. Confocal images (Leica TCS SP8) were segmented with Cellpose[48] and quantification of mean and total fluorescence intensity was done in Cellprofiler v4.2.6[49].

RT-qPCR and microfluidic RT-qPCR

Total RNA was isolated using the RNA XS Plus kit (Macherey-Nagel) and reverse transcribed using the iScript Reverse Transcription Supermix (Bio-Rad). Gene expression was quantified by SYBR-based RT-qPCR using the ΔΔCq method, normalized to reference genes (*B2M, GAPDH, RPL19*) and compared to the negative control of each experiment. Microfluidic RT-qPCR was performed in a 96x96 Dynamic Array Integrated Fluidic Circuits (Fluidigm), with 20 ng of RNA input, a 14-cycle pre-amplification and treatment with Exonuclease I. Primers and cycling conditions are described in Supplementary Methods and Supplementary Table 1.

Generation of CRISPR/Cas9 knock-out (KO) cell lines

Single guide RNAs (sgRNAs) designed to disrupt the IFNAR1, TRAF6 and MyD88 *loci* and three non-targeting control sgRNAs (Supplementary Table 2) were synthesized by Thermo Fisher Scientific. The sgRNAs (12 pmol) were complexed with 2μg of TrueCut Cas9 Protein v2 (Thermo Fisher) and delivered by electroporation (Neon Transfection System, Thermo Fisher Scientific). Genome editing was quantified using the ICE analysis tool (Synthego). Knockouts were validated at the protein level by confocal microscopy (IFNAR1 and MyD88). Functional validation was performed per target; *IFNAR1*-KO by loss of IFN-α-induced (10 IU/mL) STAT2 nuclear translocation, and *TRAF6*-KO by loss of NF-κB p65 nuclear translocation after FLAMOD stimulation (100 ng/mL).

Co-immunoprecipitation and Western blotting

T3 cells were stimulated with porcine IFN-α (10 UI/mL) for 30 min with or without FLAMOD (100 ng/mL), lysed and endogenous MyD88 was immunoprecipitated (anti-MyD88, clone B-1, Santa Cruz Biotechnology). Inputs and eluates were resolved by SDS-PAGE, transferred to nitrocellulose and probed for MyD88 and JAK1with chemiluminescence detection.

Pig infection model

Experiments were performed at the INRAE-PFIE platform under ethics approval APAFIS #43578-2023051616364291. Fifteen 4-week-old SIAV-seronegative large white pigs were randomized, and balanced for sex into three groups: mock-infected controls (n = 3), $H1_{av}N2$-infected pigs treated with vehicle (NaPi buffer; n = 6), and $H1_{av}N2$-infected pigs treated with FLAMOD (n = 6). Pigs were inoculated intratracheally with 2×10^6 $TCID_{50}$ of the $H1_{av}N2$ or PBS. One-hour after inoculation, infected pigs received 1.3 mg of FLAMOD or NaPi buffer using an Aerogen mesh nebulizer system. Animals were monitored over 72 h by blinded observers; clinical signs (increased respiratory frequency, irregular breathing, cough, lethargy, reduced mobility) were scored as binary events (cumulative score 0–5). Serum CRP (0, 24, 72 h) was measured using a Pig CRP ELISA Kit (Bio-Techne).

Single-nucleus RNA-seq sample preparation

Adjacent right cranial lobe sections were used for snRNA-seq and viral titration. Nuclei were isolated by Dounce homogenization in citric acid-sucrose buffer as previously described[50]. snRNA-seq libraries were prepared using the Chromium GEM-X Single Cell 3' reagent kit v4 according to the manufacturer's protocol with a target capture of 20000 nuclei per sample and sequenced on Illumina NextSeq 2000.

Single-nucleus RNA-seq data processing and cell type annotation

Raw sequencing reads were aligned to a combined reference comprising the Sus scrofa Sscrofa11.1 pig genome and the eight genomic segments of A/swine/France/35-200154/2020 (H1N2 strain; GenBank accessions MZ088854–MZ088861) using Cell Ranger v9.0.1 (10x Genomics). Downstream analysis was performed using Seurat v5.4.0. Doublet identification and donor demultiplexing were performed using Demuxafy v3.0.0 (DoubletFinder, scds, scDblFinder, Souporcell, and Vireo). Ambient RNA was removed using decontX (celda R package v1.26.0). Nuclei in the bottom and top 5^{th} percentiles of detected genes and mitochondrial transcript fraction ≥5% of total UMI counts were excluded. After filtering, 135,349 cells were retained. Counts were normalized using SCTransform and PCA was performed on the top 3,000 most variable host genes (excluding viral genes) before CCA-based integration. Clusters were identified using the Louvain algorithm at resolution 0.6, yielding 30 populations annotated by canonical markers.

Module scoring, meta-analysis and differential expression gene (DEG)

Type I IFN expression and type I and type II ISG module scores were computed per cell using pig type I IFN paralogs and the MSigDB Hallmark Interferon Alpha and Interferon Gamma gene sets with the Seurat v5 AddModuleScore function. For all treatment comparisons, cells were stratified by infection state (bystander, low, high viral load) and aggregated to donor-level pseudobulk (n = 6 per group). ISG scores were compared by a two-stage REML random-effects meta-analysis across cell types (R package metafor). Heterogeneity was quantified as I^2. A sign test (exact binomial, one-sided) was applied to assess whether the direction of effect was consistent across cell types.

Pseudobulk DEG analysis was modeled with DESeq2 with significance defined as FDR < 0.05. Genes were ranked by Wald statistic and tested for ISG enrichment by pre-ranked GSEA (fgsea; FDR < 0.05).

Statistics and Reproducibility

Statistical analyses were performed using R v4.4.3 (packages lmerTest, emmeans, drc, mclust, DESeq2, metafor and Seurat). Statistical details for each experiment are provided in the corresponding figure legends. Assumptions of normality and homogeneity of variance were evaluated prior to applying the appropriate statistical test. Two group comparisons used Student's *t*-test or the Mann–Whitney U test. Multiple groups were compared using one-way, two-way or three-way analysis of variance (ANOVA); for one-way designs, ANOVA was followed by Tukey's HSD post hoc test for pairwise comparisons. Knockout RT-qPCR was modeled by linear mixed-effects models (treatment x genotype as fixed effect, experimental day as random intercept). Longitudinal serum CRP concentrations were analyzed by a linear mixed-effects model on log-transformed values (treatment x day and their interaction as fixed effects and pig as random) intercept. STAT2 dose-response curves were fitted to a four-parameter log-logistic model. All snRNA-seq data was analyzed at the donor pseudobulk level. Alpha was set to 0.05. Unless otherwise stated, results are presented as individual data points with horizontal bars indicating the mean ± SEM.

Detailed materials and methods are described in the data supplement.

Data availability

The snRNA-seq datasets generated during the current study are available in the GEO repository with GEO accession number GSE346791. Reviewers must enter token kxangwoqnrklhsd into the box to access the data.

Code availability

No custom code was developed for this study. All analyses were performed using publicly available software and R packages as described in the Methods.

REFERENCES

1. Deblanc, C. & Simon, G. Involvement of swine influenza A viruses in the porcine respiratory disease complex. *Virologie (Montrouge)* **21**, 225–238 (2017).
2. Deblanc, C. *et al.* Mycoplasma hyopneumoniae does not affect the interferon-related anti-viral response but predisposes the pig to a higher level of inflammation following swine influenza virus infection. *J Gen Virol* **97**, 2501–2515 (2016).
3. Anderson, T. K. *et al.* Swine Influenza A Viruses and the Tangled Relationship with Humans. *Cold Spring Harb Perspect Med* **11**, a038737 (2021).
4. Coggon, A. *et al.* Quantifying the zoonotic risk profile of European influenza A viruses in swine from 2010 to 2020 inclusive. *J Virol* **99**, e00306-25 (2025).

5. Petro-Turnquist, E., Pekarek, M. J. & Weaver, E. A. Swine influenza A virus: challenges and novel vaccine strategies. *Front. Cell. Infect. Microbiol.* **14**, 1336013 (2024).
6. Parys, A., Vandoorn, E., Chiers, K. & Van Reeth, K. Alternating 3 different influenza vaccines for swine in Europe for a broader antibody response and protection. *Vet Res* **53**, 44 (2022).
7. Takeuchi, O. & Akira, S. Pattern recognition receptors and inflammation. *Cell* **140**, 805–820 (2010).
8. Hancock, R. E. W., Nijnik, A. & Philpott, D. J. Modulating immunity as a therapy for bacterial infections. *Nat Rev Microbiol* **10**, 243–254 (2012).
9. Iwasaki, A. & Pillai, P. S. Innate immunity to influenza virus infection. *Nat Rev Immunol* **14**, 315–328 (2014).
10. Matarazzo, L. *et al.* Neutrophil subsets enhance the efficacy of host-directed therapy in pneumococcal pneumonia. *Mucosal Immunol* S1933-0219(24)00117-X (2024) doi:10.1016/j.mucimm.2024.11.009.
11. Baldry, M. *et al.* Flagellin nebulization enhances respiratory immune responses in the porcine model. *iScience* **28**, 114218 (2025).
12. López-Gálvez, R. *et al.* Airway Administration of Flagellin Regulates the Inflammatory Response to Pseudomonas aeruginosa. *Am J Respir Cell Mol Biol* **65**, 378–389 (2021).
13. Vijayan, A., Rumbo, M., Carnoy, C. & Sirard, J.-C. Compartmentalized Antimicrobial Defenses in Response to Flagellin. *Trends in Microbiology* **26**, 423–435 (2018).
14. Van Maele, L. *et al.* Airway structural cells regulate TLR5-mediated mucosal adjuvant activity. *Mucosal Immunol* **7**, 489–500 (2014).
15. Barbin, G. *et al.* Local tolerance and innate immune activation of primary human respiratory cells exposed to flagellin. Preprint at https://doi.org/10.64898/2025.12.19.695341 (2025).
16. Costa, C. *et al.* Triggering Toll-Like Receptor 5 Signaling During Pneumococcal Superinfection Prevents the Selection of Antibiotic Resistance. *The Journal of Infectious Diseases* **230**, e1126–e1135 (2024).
17. Porte, R. *et al.* A Toll-Like Receptor 5 Agonist Improves the Efficacy of Antibiotics in Treatment of Primary and Influenza Virus-Associated Pneumococcal Mouse Infections. *Antimicrob Agents Chemother* **59**, 6064–6072 (2015).
18. Munoz, N. *et al.* Mucosal administration of flagellin protects mice from Streptococcus pneumoniae lung infection. *Infect Immun* **78**, 4226–33 (2010).

19. Georgel, A. F. *et al.* Toll-like receptor 5 agonist flagellin reduces influenza A virus replication independently of type I interferon and interleukin 22 and improves antiviral efficacy of oseltamivir. *Antiviral Res* **168**, 28–35 (2019).
20. Balka, K. R. & De Nardo, D. Understanding early TLR signaling through the Myddosome. *Journal of Leukocyte Biology* **105**, 339–351 (2019).
21. Kang, W. *et al.* Flagellin-Stimulated Production of Interferon-β Promotes Anti-Flagellin IgG2c and IgA Responses. *Mol Cells* **43**, 251–263 (2020).
22. Song, L. *et al.* Transcriptome Sequencing Reveals Salmonella Flagellin Activation of Interferon-β-Related Immune Responses in Macrophages. *CIMB* **45**, 2798–2816 (2023).
23. Schmitz, M. L., Kracht, M. & Saul, V. V. The intricate interplay between RNA viruses and NF-kappaB. *Biochim Biophys Acta* **1843**, 2754–2764 (2014).
24. Schneider, W. M., Chevillotte, M. D. & Rice, C. M. Interferon-Stimulated Genes: A Complex Web of Host Defenses. *Annu. Rev. Immunol.* **32**, 513–545 (2014).
25. Nempont, C. *et al.* Deletion of Flagellin's Hypervariable Region Abrogates Antibody-Mediated Neutralization and Systemic Activation of TLR5-Dependent Immunity. *The Journal of Immunology* **181**, 2036–2043 (2008).
26. Richard, G. *et al.* Major change in swine influenza virus diversity in France owing to emergence and widespread dissemination of a newly introduced H1N2 1C genotype in 2020. *Virus Evolution* **11**, veae112 (2025).
27. Biedma, M. E. *et al.* Recombinant flagellins with deletions in domains D1, D2, and D3: Characterization as novel immunoadjuvants. *Vaccine* **37**, 652–663 (2019).
28. Pfeffer, L. M. The Role of Nuclear Factor κB in the Interferon Response. *Journal of Interferon & Cytokine Research* **31**, 553–559 (2011).
29. Platanitis, E. *et al.* A molecular switch from STAT2-IRF9 to ISGF3 underlies interferon-induced gene transcription. *Nat Commun* **10**, 2921 (2019).
30. Schindler, C., Levy, D. E. & Decker, T. JAK-STAT Signaling: From Interferons to Cytokines. *Journal of Biological Chemistry* **282**, 20059–20063 (2007).
31. Denz, P. J. *et al.* Innate immune control of influenza virus interspecies adaptation via IFITM3. *Nat Commun* **15**, 9375 (2024).
32. Perkins, D. J. & Vogel, S. N. Space and time: New considerations about the relationship between Toll-like receptors (TLRs) and type I interferons (IFNs). *Cytokine* **74**, 171–174 (2015).

33. Noppert, S. J., Fitzgerald, K. A. & Hertzog, P. J. The role of type I interferons in TLR responses. *Immunol Cell Biol* **85**, 446–457 (2007).
34. Zhang, B. *et al.* Prevention and cure of rotavirus infection via TLR5/NLRC4–mediated production of IL-22 and IL-18. *Science* **346**, 861–865 (2014).
35. Hossain, M. S., Ramachandiran, S., Gewirtz, A. T. & Waller, E. K. Recombinant TLR5 Agonist CBLB502 Promotes NK Cell-Mediated Anti-CMV Immunity in Mice. *PLoS ONE* **9**, e96165 (2014).
36. Bacsik, D. J. *et al.* Influenza virus transcription and progeny production are poorly correlated in single cells. *eLife* **12**, RP86852 (2023).
37. Rabouw, H. H. *et al.* Live-cell single-vRNP imaging identifies viral gene expression signatures that shape influenza infection heterogeneity. *Cell Systems* **17**, 101489 (2026).
38. Brooke, C. B. *et al.* Most Influenza A Virions Fail To Express at Least One Essential Viral Protein. *J Virol* **87**, 3155–3162 (2013).
39. Sakuma, C. *et al.* Pig lacks functional NLRC4 and NAIP genes. *Immunogenetics* **69**, 125–130 (2017).
40. Zhou, Z. *et al.* TLR5 Signaling Ameliorates Liver Fibrosis by Inducing Interferon β-Interleukin-1 Receptor Antagonist in Mice. *SSRN Journal* https://doi.org/10.2139/ssrn.3320129 (2019) doi:10.2139/ssrn.3320129.
41. Fitzgerald, K. A. & Kagan, J. C. Toll-like Receptors and the Control of Immunity. *Cell* **180**, 1044–1066 (2020).
42. Wei, J. *et al.* The Ubiquitin Ligase TRAF6 Negatively Regulates the JAK-STAT Signaling Pathway by Binding to STAT3 and Mediating Its Ubiquitination. *PLoS ONE* **7**, e49567 (2012).
43. Wu, J. *et al.* A MyD88–JAK1–STAT1 complex directly induces SOCS-1 expression in macrophages infected with Group A Streptococcus. *Cell Mol Immunol* **12**, 373–383 (2015).
44. Matarazzo, L. *et al.* Therapeutic Synergy Between Antibiotics and Pulmonary Toll-Like Receptor 5 Stimulation in Antibiotic-Sensitive or -Resistant Pneumonia. *Front. Immunol.* **10**, 723 (2019).
45. Andersen-Nissen, E. *et al.* Evasion of Toll-like receptor 5 by flagellated bacteria. *Proc. Natl. Acad. Sci. U.S.A.* **102**, 9247–9252 (2005).
46. Gewirtz, A. T. *et al. Helicobacter pylori* Flagellin Evades Toll-Like Receptor 5–Mediated Innate Immunity. *J INFECT DIS* **189**, 1914–1920 (2004).
47. Biedma, M. E. *et al.* Recombinant flagellins with deletions in domains D1, D2, and D3: Characterization as novel immunoadjuvants. *Vaccine* **37**, 652–663 (2019).

48. Stringer, C., Wang, T., Michaelos, M. & Pachitariu, M. Cellpose: a generalist algorithm for cellular segmentation. *Nat Methods* **18**, 100–106 (2021).

49. Stirling, D. R. *et al.* CellProfiler 4: improvements in speed, utility and usability. *BMC Bioinformatics* **22**, 433 (2021).

50. Caballero, I. *et al.* Cystic fibrosis alters the structure of the olfactory epithelium and the expression of olfactory receptors affecting odor perception. *Sci. Adv.* **11**, eads1568 (2025).

Acknowledgments

We thank Alain Deslis et Noémie Perrot from the PFIE, UE-1277, INRAE Centre de Recherche Val de Loire, France for their assistance in the animal experimental trial. We thank Juliane Bruemmer, Helena Hazeu, Lisa Fischer and Michelle Michelhans for their contributions to snRNA-seq data analyses during earlier phases of the project. We additionally thank Juliane Bruemmer for her contributions to d-fine project coordination. The H3N2-Bissendorf03 strain (A/Swine/Bissendorf/IDT1864/2003) was kindly provided by Ralf Dürrwald, IDT Biologika GmbH (Dessau-Rosslau, Germany). The $H1_{av}N2$ strain (A/Swine/35-200154/2020; HA-1C.2.4) was kindly provided by the ANSES National Reference Laboratory for Swine Influenza (ANSES Ploufragan-Plouzané-Niort).

This work has been funded by the following projects: ANR Carnot France Futur Elevage, grant PIGFLU (I.C.). European Union's Horizon Europe Project 101136346 EUPAHW-SOA20 (I.C.). Views and opinions expressed are however those of the author(s) only and do not necessarily reflect those of the European Union or the European Research Executive Agency. Neither the European Union nor the granting authority can be held responsible for them. UCA GenomiX (Nice) is supported by the France 2030 program [ANR-23-IAHU-0007 (P.B.); ANR-21-ESRE- 0052 (P.B.); ANR-19-P3IA-0002 (P.B.); ANRS-23-PEPR-MIE-0003 (P.B.); ANR-10-INBS-09-03 (P.B.)]. Its support by Conseil départemental 06 (P.B.) is also acknowledged.

Author contributions:

Conceptualization: G.S., S.T., F.R., I.C.
Methodology: E.C., I.F., I.P., C.B., J.P., L.G., M.C., I.C.
Software: I.P., S.E., I.S., L.G., I.C.
Validation: E.C., I.F., I.P., I.C.
Formal analysis: E.C., I.F., I.P., I.C.
Investigation: E.C., I.F., V.G., E.K., C.B., J.P.
Resources: P.B., J.C.S., F.R., S.T., I.C.
Data Curation: E.C., I.P., L.G., I.C.
Writing – Original draft: I.C.
Writing – Review & Editing: I.P., G.S., P.B., J.C.S., F.R., S.T., I.C.
Visualization: E.C., I.P., I.C.
Supervision: F.R., S.T., I.C.
Project administration: I.C.
Funding acquisition: I.C., P.B.

Competing interests: J.C.S. is the inventor of the patents WO2009156405, WO2011161491, and WO2015011254 that describes the use of recombinant flagellin as biologic against infectious diseases and the patent WO2023275292 on the formulation of FLAMOD. All other authors declare they have no competing interests.

Ethics declarations: All experimental procedures involving animals were evaluated by the local ethics committee (Comité d'éthique en expérimentation animale Val de Loire, CEEA) and approved by the Ministry of Higher Education and Research (APAFIS #43578-2023051616364291).

Supplementary Files

This is a list of supplementary files associated with this preprint. Click to download.

- ChkhaydemetalCommBiolsupplementarymaterials.pdf
- MYD88.tif
- JAK1.tif